

STM study of surface reconstructions of Si(111):B

T.-C. Shen, C. Wang, J. W. Lyding, and J. R. Tucker

Department of Electrical and Computer Engineering and Beckman Institute, University of Illinois at Urbana-Champaign, Urbana, Illinois 61801

(Received 26 January 1994; revised manuscript received 3 May 1994)

The scanning tunneling microscope is used to study the boron-doped Si(111) surface as a function of annealing times and temperatures. The surface structure is found to be determined by the concentration of B. When the substitutional B concentration is less than 1% of the top 1×1 bilayer atoms, the surface is largely 7×7 but surrounded by adatom-covered 1×1 regions (which have higher B concentration). When the B concentration is more than 3%, the whole surface will be adatom-covered 1×1 regions including $(\sqrt{3}\times\sqrt{3})R30^\circ$ structures. The $(\sqrt{3}\times\sqrt{3})R30^\circ$ domains will increase with the B concentration. Because 7×7 can only exist in the region with low B concentration, the growth of 7×7 is slowed down. Further annealing at 560°C can convert 2×2 , $c(4\times 2)$ into 7×7 and 9×9 . Sides of the 7×7 domain preferentially grow along the three equivalent $[11\bar{2}]$ directions. The adatom-covered 1×1 regions are bounded by faulted halves of the 7×7 domains. The dark sites of 7×7 are observed and counted. They are further interpreted in terms of a B substitution model. The pattern of bright and dark atoms in $(\sqrt{3}\times\sqrt{3})R30^\circ$ domains is analyzed and a criterion for a B stabilized Si- $(\sqrt{3}\times\sqrt{3})R30^\circ$ structure is obtained.

I. INTRODUCTION

Dopant effects on semiconductor surfaces are of interest both from the scientific and technological points of view. Boron has been a common dopant for silicon wafers, and the reconstruction of the Si(111) surface with the absorption of boron has been reported by several authors in recent years. The well-known $(\sqrt{3}\times\sqrt{3})R30^\circ$ reconstruction, similar to cases of depositing other group-III elements, has been determined by low-energy electron diffraction (LEED), reflection high-energy electron diffraction (RHEED), and Auger electron spectroscopy (AES).^{1,2} However, the peculiar atomic arrangement of boron, distinguishing itself from other group-III elements on the Si(111) surface, was not determined until later works with x-ray diffraction,³ angle-resolved photoemission and inverse photoemission,⁴ LEED,⁵ and scanning tunneling microscopy (STM) with a total-energy calculation.^{6,7} It has been found that due to the shorter Si-B bond length, the most stable configuration occurs when each boron atom occupies a substitutional site directly underneath a silicon adatom at a T_4 site. Therefore, all surface $(\sqrt{3}\times\sqrt{3})R30^\circ$ adatoms are Si, and the saturated substitutional B concentration would be 16.7% of the top bilayer Si atoms [or $\frac{1}{3}$ monolayer (ML) defined by the top layer of the bulk 1×1 cell]. This is much higher than the bulk concentration even for highly doped Si wafers (e.g., the doping level of $2\times 10^{19}/\text{cm}^3$ corresponds to 0.47% of the bilayer atoms). Since the boron-rich surface reconstruction is $(\sqrt{3}\times\sqrt{3})R30^\circ$ instead of 7×7 , one can conclude that the lowest-energy surface structure with the presence of boron should be the $(\sqrt{3}\times\sqrt{3})R30^\circ$ reconstruction. Therefore, one would expect more boron atoms to be attracted to the Si surface as the sample is annealed longer or with higher temperature.

Knowing the two limits (B free and B saturated) of the B/Si(111) surface reconstruction leads naturally to questions about the surface structure at intermediate B concentration. Korobtsov, Lifshits, and Zotov¹ observed the transition of the LEED pattern from 7×7 to 1×1 to $(\sqrt{3}\times\sqrt{3})R30^\circ$ as the boron surface concentration increases with annealing time. However, LEED only reveals the averaged surface symmetry without real-space atomic structure identification. Previous STM studies^{6,7} indeed show a mixture of 7×7 and $(\sqrt{3}\times\sqrt{3})R30^\circ$ structures in small scales when the boron concentration is low, but make no determination of the pattern of large-scaled structure. It remains unclear how the surface structure changes from 7×7 to $(\sqrt{3}\times\sqrt{3})R30^\circ$ when boron atoms reach the surface, and how the presence of boron affects the growth of the domains of 7×7 from 1×1 around and below 860°C where the 1×1 to 7×7 phase transition occurs.⁸ These questions are interesting because the transition mechanism involves not only the stress and energy of various structures, but also their growth dynamics from the initial state and the availability of adatoms. In other words, intermediate states can play an important role in determining the surface structure. We approach these questions by using highly doped Si samples annealed with various temperatures and times to control the surface boron concentration and the dynamical process of surface structure growth, prior to room-temperature STM studies. These studies show that when the surface boron density is below about 2%, regions of mixed adatom-covered 1×1 structure, including 2×2 , $c(4\times 2)$, $(\sqrt{3}\times\sqrt{3})R30^\circ$, and the dimer-adatom-stacking-fault (DAS) structures, form between 7×7 domains. Following the notation of Ref. 9, these adatom-covered 1×1 regions will be denoted by $a/1\times 1$ hereafter. If the boron surface concentration is about 2%

of the top bilayer atoms, DAS structure can only grow near the upper step edge, while the rest of the surface is $a/1 \times 1$. When the surface B density is beyond 3%, no 7×7 can be found and the whole surface will be $a/1 \times 1$ and $(\sqrt{3} \times \sqrt{3})R 30^\circ$ reconstructed. The size of the $(\sqrt{3} \times \sqrt{3})R 30^\circ$ domains will then grow with the surface B concentration. Since the $a/1 \times 1$ region gives 1×1 LEED pattern, these observations explain the LEED pattern transition from 7×7 to $(\sqrt{3} \times \sqrt{3})R 30^\circ$. From the annealing time and temperature dependence of the surface structure pattern, several properties of the 7×7 domain growth and the energy relations among these surface structures can be deduced.

II. EXPERIMENTAL DETAILS

The tunneling microscope used in this work has been described elsewhere.¹⁰ The STM is housed in a two-chamber UHV system. The STM chamber (base pressure of 7×10^{-11} Torr) is connected to a sample preparation chamber (base pressure 1×10^{-10}) equipped with resistive heating, gas dosing, and LEED. Si(111) samples were from 0.030-in-thick *p*-type (B doped) and *n*-type (As doped) wafers with resistivity of 0.005 or 0.1 Ω cm, from Virginia Semiconductor, Inc. The samples were chemically cleaned by the RCA (Ref. 11) method, then degassed in the sample preparation chamber overnight at 600°C by dc current resistive heating. Oxide and hydrocarbon contaminants were removed by flashing several times to 1280°C for a few seconds. Final sample preparation was accomplished either by radiation quenching or annealing. Radiation quenching with an initial cooling rate of about 200°C/s was accomplished by switching off dc current after the 1280°C flashing. Annealed samples with different surface structure were prepared by dc resistive heating from 2 min to 1 h at temperatures ranging from 510 to 1000°C, followed by slow cooling (about 1°C/s) to room temperature. After sample annealing, we used LEED to characterize the sample surface before transferring it into the STM chamber. The sample temperature was measured with a Wahl DHS-52 infrared pyrometer (emissivity setting at 0.7) calibrated by thermocouple at low temperatures, and a tube oven at high temperatures. Tips were made by dc etching 0.25-mm-diameter W wires in 2N NaOH solution, followed by a few hours of degassing by resistive heating in the sample preparation chamber. All STM images presented here were obtained at a constant current of 0.1 nA and at sample biases of ± 1 to ± 2 V. Images are shown with a conventional gray scale keyed to the surface height.

III. RESULTS

Figure 1(a) shows a typical result for a highly doped *p*-type sample (resistivity 0.005 Ω cm) radiation quenched from 1280°C. There are many 7×7 domains of various sizes surrounding darker triangular regions. These darker regions with brighter protrusions are the areas containing a mixture of simple adatom structures like 2×2 , $c(4 \times 2)$, $(\sqrt{3} \times \sqrt{3})R 30^\circ$ and small patches of DAS structures like 7×7 and 9×9 . Similar to the laser-

stabilized Si(111) surface,¹² it is this mixed symmetry that gives the 1×1 LEED pattern. The bright protrusions contribute to the LEED background. The overall LEED pattern will be a mixture of 1×1 and 7×7 depending on the ratio between the 7×7 domain and the $a/1 \times 1$ region. The observation that the 7×7 structure is preferred at the upper step edge, even with the presence of

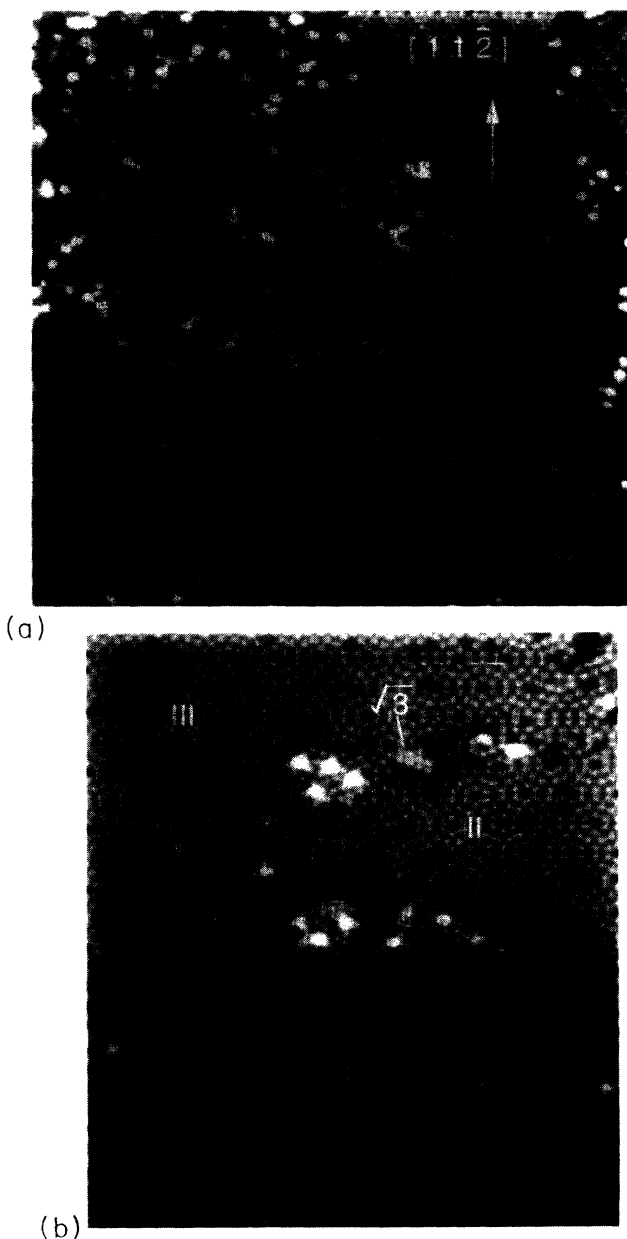


FIG. 1. STM images of a quenched Si(111) surface with high-B doping ($2 \times 10^{19}/\text{cm}^3$). (a) A $600 \times 600\text{-}\text{\AA}^2$ occupied-state image taken at sample bias -1 V. The $a/1 \times 1$ regions appear darker. A patch of 7×7 bounded by faulted halves has grown in the middle of the $a/1 \times 1$ region. The area of $a/1 \times 1$ region is about 31%. (b) A $355 \times 400\text{-}\text{\AA}^2$ unoccupied-state image taken at sample bias 1.5 V. A small triangular-shaped $a/1 \times 1$ region with a mixture of 2×2 , $c(4 \times 2)$, and $(\sqrt{3} \times \sqrt{3})R 30^\circ$ structures forms between the three domains of 7×7 (denoted by I, II, and III). The density of darker adatoms, marked by D, are about 0.5% in the 7×7 region.

boron, agrees with high-temperature STM data⁸ that 7×7 grows from the upper step edge from the 1×1 phase for the pure Si case. Nevertheless, 7×7 regions are not limited to domains bounded by the step edge. There are many 7×7 domains in the interior as well. Apparently, cooling the sample below the 1×1 – 7×7 transition temperature leads to the simultaneous nucleation of many 7×7 domains. One can notice that the 7×7 regions are almost always bounded by the faulted halves of the unit cell, so the $a/1\times 1$ regions are a union of all the equilateral triangles pointing along the $[11\bar{2}]$ direction. DAS 7×7 , 9×9 , and 11×11 (not shown) can also grow inside the $a/1\times 1$ region. We observe that if a single subunit of a DAS structure forms in the $a/1\times 1$ region, it will be the faulted half of the unit cell even though the unfaulted half has been argued to have lower energy.¹³ The bright protrusions are randomly distributed all over the $a/1\times 1$ region but never in 7×7 domains. Figure 1(b) shows an unoccupied-state image of a small $a/1\times 1$ region containing small patches of 2×2 , $c(4\times 2)$, and $(\sqrt{3}\times\sqrt{3})R30^\circ$. Comparing this with the occupied-state images, we confirm the conclusions of Becker *et al.*¹⁴ that the occupied-state image shows smaller contrast than the unoccupied-state image and the position of Si protrusions do not superimpose due to the charge transfer from the adatoms to rest atoms for the 2×2 and $c(4\times 2)$ structures. The darker spots in the 7×7 area in the unoccupied-state images are of the same height as the darker atoms in the $a/1\times 1$ region. The $a/1\times 1$ region only forms between three or more 7×7 domains.

When the sample is subsequently annealed at 560°C for 5–30 min, the 7×7 LEED pattern is regained. STM reveals that the surface pattern of the $a/1\times 1$ region has changed drastically, as shown in Fig. 2. Comparing Figs. 1 and 2, one finds that the size of the $a/1\times 1$ region is

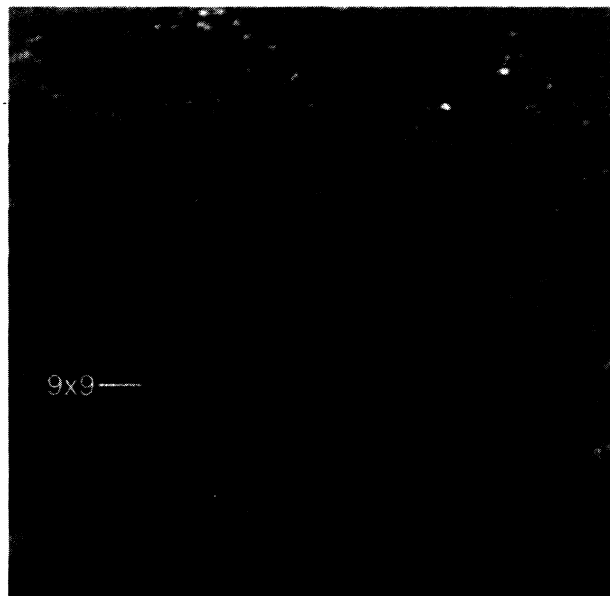


FIG. 2. A $800\times 800\text{-}\text{\AA}^2$ STM image of a Si(111) surface with high-B doping ($2\times 10^{19}/\text{cm}^3$) after flashing at 1280°C followed by annealing for 5 min at 560°C . The area of the $a/1\times 1$ region is about 17%. A patch of 9×9 is visible.

greatly reduced and the domain size of the 7×7 has increased. Associated with the 7×7 domain expansion is an increase in the $(\sqrt{3}\times\sqrt{3})R30^\circ$ structure presence in the $a/1\times 1$ regions (not shown). The bright and dark adatoms of the $(\sqrt{3}\times\sqrt{3})R30^\circ$ structure^{6,7} are noticeable, and will be discussed below. Notice that 9×9 still exists after this anneal, as shown in Fig. 2.

To find out the consequence of a higher-temperature anneal, the sample was heated to 710°C for 2 min. This resulted in further growth of the 7×7 domain size, and further reduction of the $a/1\times 1$ region area as shown in Fig. 3. The $(\sqrt{3}\times\sqrt{3})R30^\circ$ structure is now more pronounced in the $a/1\times 1$ region. Note that the bright protrusions can be resolved in this unoccupied-state image into a ringlike structure with three lobes, which leads us to suspect that they are metal contamination.^{15,16} The diameter of this ringlike structure is about 7.7 \AA , which agrees with the Ni-induced Si six-adatom clusters. The LEED pattern is still dominated by 7×7 since the $a/1\times 1$ region represents a small fraction of the surface.

With further annealing to 810°C for 2 min, the $a/1\times 1$ region aggregates into a few large areas surrounded by huge 7×7 domains, as shown in Fig. 4. The $(\sqrt{3}\times\sqrt{3})R30^\circ$ structure density in the $a/1\times 1$ region, however, is not substantially higher than the that for the 710°C annealed case. An anneal of 900°C gives rise to even larger $a/1\times 1$ regions, and much weaker seventh-order dots of the LEED pattern.

Finally we annealed the sample at 1000°C for 2 min. The LEED pattern showed a weak $(\sqrt{3}\times\sqrt{3})R30^\circ$ pattern, and STM images reveal many $(\sqrt{3}\times\sqrt{3})R30^\circ$ domains of both bright and dark adatoms with scattered 2×2 and $c(4\times 2)$ structures in between. No traces of



FIG. 3. A $450\times 450\text{-}\text{\AA}^2$ STM image of a Si(111) surface with high-B doping ($2\times 10^{19}/\text{cm}^3$) after flashing at 1280°C followed by annealing for 2 min at 710°C . The $(\sqrt{3}\times\sqrt{3})R30^\circ$ structure is more pronounced in the triangular region. The area of $a/1\times 1$ region is about 2.2%. The bright protrusions can be resolved into ringlike structures. The sample bias is +1 V.

7×7 can be found any more. One hour annealing at 1280°C makes the $(\sqrt{3}\times\sqrt{3})R30^\circ$ domains larger, as shown in Fig. 5 and, correspondingly, a sharp $(\sqrt{3}\times\sqrt{3})R30^\circ$ pattern in LEED. However, the population of dark atoms is only about 40–50 % of the $(\sqrt{3}\times\sqrt{3})R30^\circ$ domain, and less than 6% of the total top bilayer atoms.

Some of our results are summarized in Tables I and II. In Table I, we present the measurement of the percentage of the $a/1\times 1$ area from a set of experiments. These numbers were obtained from some large-scaled STM data ($2400\text{--}3000\text{ \AA}$), thanks to the great contrast between the $a/1\times 1$ and 7×7 regions in the occupied-state images. Table II lists the “atom count” in a few typical $a/1\times 1$ regions from some high-resolution small-scaled ($300\text{--}450\text{ \AA}$) data sets. The order of the entries reflects the actual sequence of a set of experiments. The third column is the extra percentage of the total number of adatoms (bright and dark) compared to the hypothetical number of 7×7 adatoms in the $a/1\times 1$ region. It is assumed that six Si adatoms are associated with each metal impurity atom and included in the total number count. A word of caution is in order. Since the B concentration on the surface

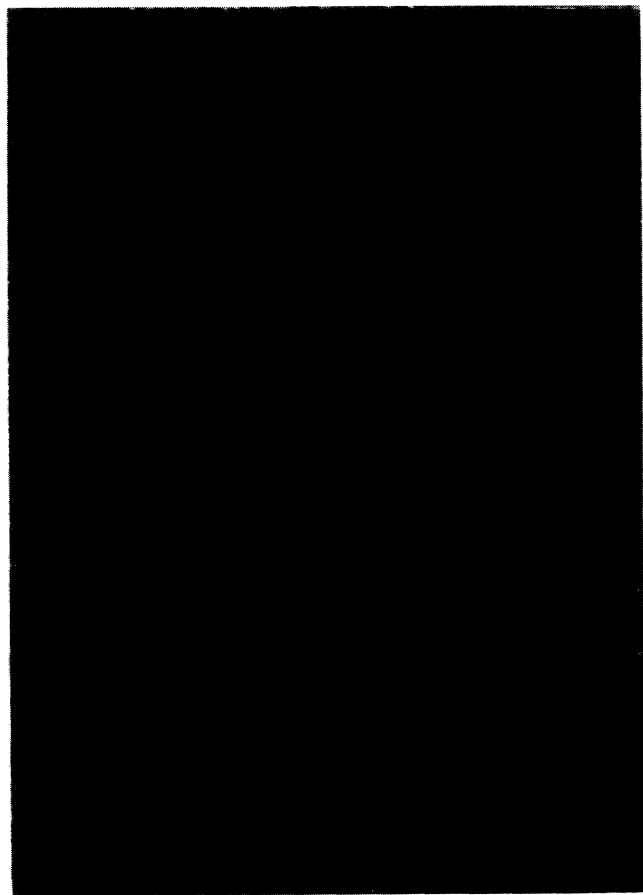


FIG. 4. A $2250\times 3000\text{-\AA}^2$ STM image of a Si(111) surface with high-B doping ($2\times 10^{19}/\text{cm}^3$) after flashing at 1280°C , followed by annealing for 2 min at 810°C . The sample bias is -1 V . The $a/1\times 1$ regions (about 8.3% in area) have aggregated into larger regions surrounded by 7×7 domains.

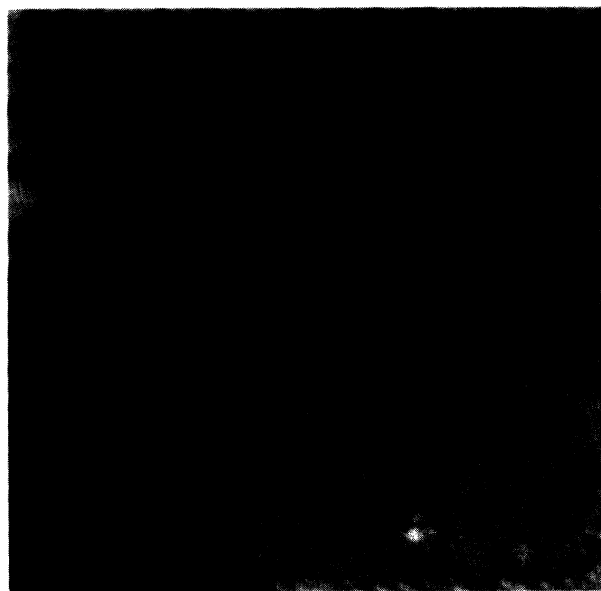


FIG. 5. A $300\times 300\text{-\AA}^2$ STM image of a Si(111) surface with high-B doping ($2\times 10^{19}/\text{cm}^3$) after annealing for 1 h at 1280°C . The sample bias is $+1\text{ V}$. Domains of $(\sqrt{3}\times\sqrt{3})R30^\circ$ and $c(4\times 2)$ and 2×2 are visible. The dark or bright adatoms of $(\sqrt{3}\times\sqrt{3})R30^\circ$ are believed to have B or Si, respectively, underneath them. The dark atoms occupy 5–8 % of the top bilayer atoms. The row pattern is discussed in Sec. IV B.

depends on the sample preparation history (details in Sec. IV A), the numbers in these two tables are only sensible for the purpose used in our discussion.

To verify our results we prepared a moderately B-doped ($0.1\text{ }\Omega\text{ cm}$) Si(111) samples the same way as previously described. After a few seconds at 1280°C , the quenched sample shows only huge 7×7 domains over the entire terrace. The domain boundaries are decorated with a few bright protrusions are less than one 7×7 unit cell wide. The dark adatom concentration in the 7×7 area is about 0.11% compared to 0.56% for the highly doped samples (see Table II). Subsequent annealing at 1280°C for 30 min followed by quenching gives more spots in the 7×7 area, and more bright protrusions accumulated in the narrow domain boundaries. Small triangular $a/1\times 1$ regions with sides of about $2\text{--}3\text{ }7\times 7$ unit

TABLE I. The area percentage of the $a/1\times 1$ region in the total scanned area for each sample preparation. The order of the entries is chosen to follow the actual sequence of a set of experiments because the surface B density depends on the history of sample preparation. These numbers are obtained from $2400\text{--}3000\text{-\AA}$ -wide occupied-state STM data sets.

Sample preparation	Area of $a/1\times 1$ (%)
710°C -2 min	2.2–3.7
710°C -5 min	4.1
810°C -2 min	8.3–10
quenched	52–59
560°C -5 min	17–22
510°C -5 min	46–57

TABLE II. The third column is the extra percentage of the total number of adatoms (bright and dark) compared to the hypothetical number of 7×7 adatoms in the $a/1 \times 1$ region. It is assumed that six Si adatoms are associated with each metal impurity atom and included in the total number count. The last row is the data from a moderately B-doped sample. Each $a/1 \times 1$ region is selected from a typical high resolution 300–450-Å STM unoccupied-state data set. A larger statistical variation is expected, because of the small number of data sets. The order of the entries is chosen to follow the actual experimental sequence since the surface B density depends on sample preparation history.

Sample preparation	Dark atoms in $a/1 \times 1$ (%)	Extra atoms in $a/1 \times 1$ (%)	Dark atoms in 7×7 (%)
710°C—2 min	2.7	27	0.56
710°C—5 min	4.0	28	0.68
quenched	1.6–2.0	13–19	0.76
560°C—10 min	2.1–2.5	17	0.48–0.68
510°C—5 min	1.2	15	
quenched			0.11

cells are formed between three or more 7×7 domains. Further annealing at 1280°C for 1 h generates huge clustering of the $a/1 \times 1$ region and equally huge 7×7 domains. In this case we observe that within the general outline of the $a/1 \times 1$ region defined by 7×7 domains there are more 9×9 surrounded by patches of $a/1 \times 1$ covered with many “bright” protrusions. Again, when annealed at 560°C for 10 min, the DAS region expands, leaving only the narrow domain boundaries as remnants of the $a/1 \times 1$ regions.

To separate the effect of boron from other unintentional impurities, we ran the same set of experiments with an arsenic-doped sample (resistivity 0.005 Ω cm). Similar to the moderately B-doped sample, quenching after a few seconds at 1280°C leads to nothing but uniform 7×7 regions with near unit-cell-wide domain boundaries decorated with a few bright protrusions. Even annealing the sample at 1120°C for 2.5 h followed by a 2-min anneal at 1330°C does not produce any $a/1 \times 1$ region or substantially increase of the number of 7×7 defects. Thus we believe the driving force behind these surface patterns is due to boron atoms.

IV. DISCUSSION

A. The formation of $a/1 \times 1$ region and the growth of 7×7

In order to understand the formation of the $a/1 \times 1$ region, we shall begin with the two mechanisms in our experiments that can raise the B density on the surface. The first mechanism occurs during the high-temperature flashing. Since the B evaporation rate from a silicon surface is only about 1% of that of Si,¹⁷ repeated flashing at 1280°C causes B to accumulate at the surface. A profile of B distribution after 1-h annealing at 1280°C is shown in Fig. 6. The second mechanism is B diffusion from the bulk. Using the diffusion coefficient obtained in Ref. 1,

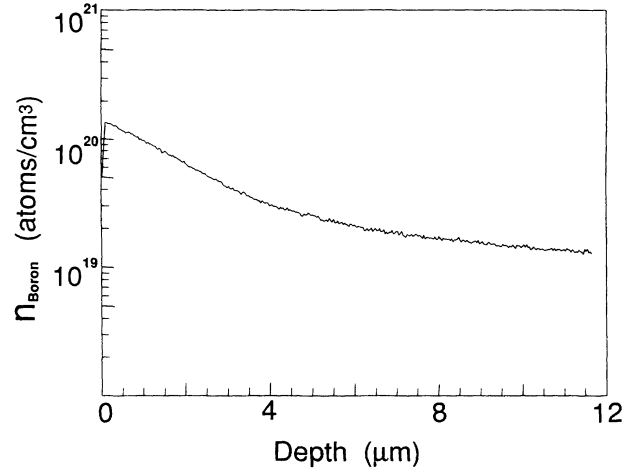


FIG. 6. The SIMS analysis of the B concentration profile of a highly B doped ($2 \times 10^{19}/\text{cm}^3$) Si(111) sample after annealing for 1 h at 1280°C.

we can estimate the diffusion lengths from the bulk over 2 min at 600, 700, and 800°C to be roughly 0.18, 2.3, and 18 Å, respectively. By comparison, the diffusion length for 1 sec at 1280°C is about 800 Å. Therefore, the bulk B diffusion is rather insignificant for our low-temperature annealing, and we can study the transition of surface structures below 600°C by assuming constant surface B concentration. However, beyond 800°C, B atoms within several layers deep may diffuse to the surface and be trapped due to the higher B “soluble” ($\sqrt{3} \times \sqrt{3}$) $R30^\circ$ structure on the surface. In general, we find that the $a/1 \times 1$ region surface coverage increases with total annealing time and temperature. For example, after 810°C annealing the $a/1 \times 1$ region area has substantially increased when compared with 700°C annealing, and the $a/1 \times 1$ region area is essentially unchanged after annealing at 560 or 510°C for either 5 or 30 min (see Table I). These results infer that the $a/1 \times 1$ region is related to the boron distribution on the surface. This point is further supported by the fact that the *n*-type sample shows no $a/1 \times 1$ region, and that the moderately B-doped sample shows a much smaller $a/1 \times 1$ area. Based on these observations and assumptions, we reach the following interpretation to our STM data. Boron on the Si surface interferes with the long-range order of the DAS structures by slowing down the 7×7 growth and leaving the simple adatom covered 1×1 structure between 7×7 domains. Additional annealing at about 560°C enhances the conversion of Si adatom structure from 2×2 and $c(4 \times 2)$ into 7×7 , so the 7×7 domains grow at the expense of reducing the $a/1 \times 1$ regions (Fig. 2). However, lower-temperature (510°C) annealing shows no such effect. Thus we can conclude that the onset temperature of the 7×7 conversion from 2×2 and $c(4 \times 2)$ in the presence of B is between 510 and 560°C. Intuitively one would expect that upon cooling from 1280°C, it is easier to form the smaller-unit-celled structures like 2×2 or $c(4 \times 2)$ than the larger-celled DAS structure which in-

volves the formation of dimers, corner holes, and stacking faults. However, it is also known that 7×7 is the lowest-energy structure on Si(111). From our observations of the expansion of the 7×7 domains and the occurrence of isolated 7×7 and 9×9 unit cells in the $a/1\times 1$ region, we can conclude that DAS structure has lower energy than 2×2 and $c(4\times 2)$, and 7×7 is still the lowest-energy structure if locally the surface B density is less than 1% (see the dark adatom density in Table II).

The 7×7 structure is preferred at the upper step edge until the whole surface has turned into $a/1\times 1$, where the surface concentration of B is about 3%. This observation can be explained by the hypothesis that the B-substituted 7×7 costs more energy to form than the pure Si 7×7 . Thus B atoms are expelled by the formation of 7×7 until the local critical density (about 2%) has reached, and the advance of 7×7 is stopped. The 7×7 or 9×9 domains inside the $a/1\times 1$ region can be as small as half a unit cell. Expitaxially, a 7×7 domain can grow in both $[\bar{1}\bar{1}2]$ and $[11\bar{2}]$ directions.¹⁸ However, on this surface our observation suggests that the growth of 7×7 is favored along $[11\bar{2}]$ directions. Therefore, one would expect the basic form of the 7×7 domain to be triangular, which is clearly demonstrated in Fig. 7. It seems reasonable for the surface to have the faulted halves at the boundary, because no extra stacking fault needs to form in the neighboring $a/1\times 1$ region in order to have a smooth connection to the 7×7 domain. Further evidence for this is obtained from the observation that all single DAS subunits in the $a/1\times 1$ region are faulted.

From some STM images, one may think that it is the metal impurities that stabilize the $a/1\times 1$ region and stop the 7×7 growth. This is possible, but cannot be the major factor to account for the surface pattern observed

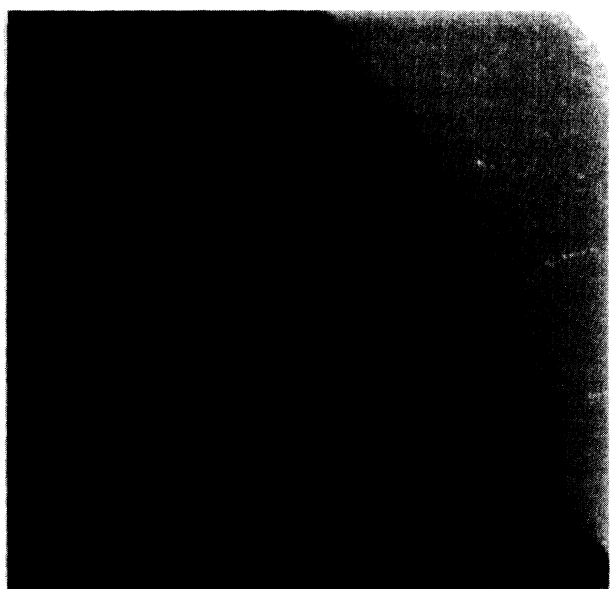


FIG. 7. A $2000\times 2000\text{-}\text{\AA}^2$ STM image of a Si(111) surface with high-B doping ($2\times 10^{19}/\text{cm}^3$) after flashing at 1250°C followed by annealing for 3 min at 700°C . The sample bias is -2 V. The triangular-shaped 7×7 domains indicate that the growth of the 7×7 domains on this surface is along the three equivalent directions of $[11\bar{2}]$.

in our experiments for the following two reasons. First, we have images of $a/1\times 1$ region with very low impurity concentration (e.g., two bright protrusions in an area of $300\times 300\text{\AA}^2$). It seems quite unlikely that so few impurity atoms can stabilize such a large area. Second, as already discussed in Sec. III, less B-doped or As-doped samples show few or no $a/1\times 1$ regions for the same sample preparation. However, it is possible that metal atoms also contribute to the slowing down of the 7×7 growth. Since they cannot form a stable substitutional structure within the 7×7 , they will diffuse on the surface until they can bond with six Si adatoms to form a ringlike structure in the $a/1\times 1$ region. When the temperature is high enough, both B and metal atoms will tend to diffuse toward the nearby $a/1\times 1$ region ahead of the advancing of 7×7 . The boron atoms can convert the local surface to $(\sqrt{3}\times\sqrt{3})R30^\circ$ structure to lower the surface energy, and metal atoms can find a sufficient supply of adatoms to form ringlike clusters with could also reduce the energy. Since the adatom density is higher for 2×2 or $c(4\times 2)$ surface than for 7×7 , the conversion to 7×7 results in extra adatoms. Eventually, when the energy gain from converting $a/1\times 1$ to 7×7 cannot balance the energy cost of the high-adatom-density configurations and the expulsion of metal atoms from the boundary, the equilibrium between the 7×7 and $a/1\times 1$ regions will be reached.

One interesting point is that we observed many patches of 9×9 inside the $a/1\times 1$ region after 560°C annealing, but none in the more open area like a step edge; while a lesser adatom-required 5×5 structure was never observed in the surrounded $a/1\times 1$ region. This is consistent with the result of Feenstra and Lutz⁹ which showed that the 5×5 to 7×7 transition occurs at 400°C in the presence of excess adatoms (e.g., the $a/1\times 1$ region). It also implies that the 9×9 can be stabilized in the adatom-rich environment up to a temperature between 560 and 710°C above which the transition to 7×7 occurs.

Recently, Yang and Williams²⁰ reported that similar surface structures can be generated by preparing very large-sized terraces on Si(111) and quenching the samples from high temperature. The idea is to make the sample cooling time shorter than that required for the adatoms to diffuse to the step edge. Since the adatom density on the terrace is higher than 7×7 , the adatom-rich structures $a/1\times 1$, 9×9 , and 11×11 can be formed. Our system is slightly more involved because of B. As discussed previously, the presence of B forces 7×7 to form only in the region with low-B density, and leaves the rest of the surface in $a/1\times 1$. Further low-temperature annealing helps the agglomeration of B to form $(\sqrt{3}\times\sqrt{3})R30^\circ$ and helps the conversion of $a/1\times 1$ to 7×7 , 9×9 , or 11×11 . The mechanism of this part is identical to that of Ref. 20; that is, lower-temperature annealings do not give Si atoms a large enough diffusion length to move to the step edge. Thus DAS structures with higher adatom densities will form.

B. Dark atoms in $(\sqrt{3}\times\sqrt{3})R30^\circ$ and 7×7

It has been pointed out^{6,7} that the darker atom in the STM images of the $(\sqrt{3}\times\sqrt{3})R30^\circ$ structure corresponds

to a B atom underneath the Si adatom. We also found similar "dark" atoms in 7×7 regions. Since the number of these dark atoms increases with annealing, we postulate that the same argument applies; that is, one B atom is associated with each dark 7×7 adatom. It has been suggested that the stability of $(\sqrt{3}\times\sqrt{3})R30^\circ$ over 7×7 is due to the charge transfer from the surface dangling bonds to the boron atoms.⁶ Since the rest-atom band will be filled first in the case of 7×7 , the adatom bands can only be partially fulfilled.¹⁹ Suppose one of the Si rest atoms in 7×7 is substituted with a B atom; there will be one electron less in the surface band associated with adatom dangling bonds. As in the case of the $(\sqrt{3}\times\sqrt{3})R30^\circ$ structure, both the occupied- and unoccupied-state STM images of these sites will be darker. In one case we found two neighboring dark adatoms in a 7×7 unit cell in an unoccupied-state image, but the corresponding occupied-state image shows only the neighboring rest atom. This is a clear demonstration of the charge-transfer effect caused by substituted B atoms. However, we have never found dark atoms in the 2×2 or $c(4\times 2)$ regions. We speculate that whenever a B atom occupies a T_4 site in the 1×1 layer, the charge transfer from the Si adatom stabilizes the next adatom to be $\sqrt{3}a$ rather than $2a$ distance away ($a=3.84\text{ \AA}$). Table II tabulates a count of dark atoms in the $a/1\times 1$ and 7×7 regions compared to the total 1×1 bilayer atoms for various sample preparations. Assuming the dark atoms represent B, the B concentration in the 7×7 region increases slightly with the annealing time and temperature. It is interesting to note that if there were one dark atom in every half- 7×7 unit cell, then there would be a 2% B substitution density in the top bilayer. The observed upper limit for a stable 7×7 configuration is, however, less than 1%. Inside the $a/1\times 1$ region, the B concentration measured by counting the number of dark $(\sqrt{3}\times\sqrt{3})R30^\circ$ atoms is higher, but below 4%. Instead of simply increasing the B density and forming more $(\sqrt{3}\times\sqrt{3})R30^\circ$ structures inside the $a/1\times 1$ region, more annealing causes the $a/1\times 1$ region to grow at the expense of 7×7 regions. When the overall B density is about 2%, DAS structures can only exist near the upper step edge, while most of the terrace is $a/1\times 1$ with substantial $(\sqrt{3}\times\sqrt{3})R30^\circ$. After an hour of annealing at 1280°C , the whole surface is $(\sqrt{3}\times\sqrt{3})R30^\circ$ and we find the surface B density is between 5 and 8%. For comparison, the two-dimensional B density of the top 1000 Å estimated by secondary ion mass spectroscopy (SIMS) is about 1.4%, as shown in Fig. 6. This is a clear demonstration of the surface segregation effect. A more convincing identification of the dark atoms of 7×7 would be from the result of tunneling spectroscopy, which will be the subject of future publication. It is interesting to note that the largest array of bright $(\sqrt{3}\times\sqrt{3})R30^\circ$ structure is three consecutive rows in any direction, and is very rare (see Fig. 5). This observation implies that each Si adatom needs at least one B at a T_4 site $\sqrt{3}a$ ($a=3.84\text{ \AA}$) away to be stable. Because of this criterion, we can understand why row patterns are preferred for both bright and dark atoms in the $(\sqrt{3}\times\sqrt{3})R30^\circ$ configuration. As the surface B concentration increases, the patches of dark

(B) atoms grow larger, but the bright (Si) atoms still remain in the form of rows with a maximum width of two rows.

V. CONCLUSION

We have used the scanning tunneling microscope to study the Si(111) surface in the presence of B. We have found that high-temperature quenching leads to forming 7×7 only in the regions with less than 1% of B concentration, and leaves the rest of the surface in adatom-covered 1×1 ($a/1\times 1$). The higher the surface B concentration, the larger the area of the $a/1\times 1$ regions. This surface gives rise to the observed 1×1 LEED pattern. The dark atoms in 7×7 were interpreted as B substitutional sites. The number of dark atoms increases with annealing time and temperature. The dark atom density in 7×7 is observed to be less than 1%. Annealing at 560°C enhances the transformation from $a/1\times 1$ to 7×7 , and increases the dark atom density in the $a/1\times 1$ region to be about 2.5%. Higher-temperature annealing increases the diffusion of bulk B to the surface, and thus increases the $(\sqrt{3}\times\sqrt{3})R30^\circ$ density in the $a/1\times 1$ region. However, the dark atom density in the $a/1\times 1$ remains below 4%. As a result, the area of $a/1\times 1$ region has to be increased. The nucleation of 7×7 occurs preferentially at the upper step edge, until the surface B concentration reaches about 3%, where the whole surface is $a/1\times 1$. Small regions of $(\sqrt{3}\times\sqrt{3})R30^\circ$ with 2×2 and $c(4\times 2)$ can be found on this surface which give faint $(\sqrt{3}\times\sqrt{3})R30^\circ$ LEED patterns. Further annealing at 1280°C gives rise to a sharper $(\sqrt{3}\times\sqrt{3})R30^\circ$ LEED pattern. STM images show larger domains of $(\sqrt{3}\times\sqrt{3})R30^\circ$, and the dark atom concentration is about 5–8%. It is noted that in the $(\sqrt{3}\times\sqrt{3})R30^\circ$ structure every bright adatom must neighbor at least one dark adatom to be stable, which can be explained by the mechanism of charge transfer from the Si adatom to the B atom.

In general, we found that the DAS structure has lower energy than the 2×2 or $c(4\times 2)$. Thus 7×7 or 9×9 can be formed inside of an $a/1\times 1$ region. The 7×7 structure is still the lowest energy structure if the local B concentration is less than 1%. The transition temperature from 9×9 to 7×7 is between 560 and 710°C , and the transition from $a/1\times 1$ to 7×7 occurs between 510 and 560°C . Sides of the 7×7 domain grow preferentially along the three equivalent $[11\bar{2}]$ directions, until the energy gain from converting the $a/1\times 1$ to 7×7 no longer balances the energy cost of higher adatom density in the $a/1\times 1$ region and the expulsion of metal atoms from the boundary. Thus the $a/1\times 1$ regions are bounded by faulted halves of the 7×7 domains. The minimum size of a 7×7 or 9×9 domain in an $a/1\times 1$ region is a faulted half of the unit cell.

ACKNOWLEDGMENTS

Helpful discussions with Paul von Allmen, David G. Cahill, and Gert Ehrlich during the course of this work are gratefully acknowledged. This work is supported by

the Office of Naval Research University Research Initiative under Grant No. N00014-92-J-1519. SIMS analysis was carried out in the Center for Microanalysis of Materials, University of Illinois, which is supported by the U.S. Department of Energy under Grant No. DEFG02-91-ER45439.

-
- ¹V. V. Korobtsov, V. G. Lifshits, and A. V. Zotov, *Surf. Sci.* **195**, 466 (1988).
²H. Hirayama, T. Tatsumi, and N. Aizaki, *Surf. Sci.* **193**, L47 (1988).
³R. L. Headrick, I. K. Robinson, E. Vlieg, and L. C. Feldman, *Phys. Rev. Lett.* **63**, 1253 (1989).
⁴Efthimios Kaxiras, K. C. Pandey, F. J. Himpsel, and R. M. Tromp, *Phys. Rev. B* **41**, 1262 (1990).
⁵H. Huang, S. Y. Tong, J. Quinn, and F. Jona, *Phys. Rev. B* **41**, 3276 (1990).
⁶P. Bedrossian, R. D. Meade, K. Mortensen, D. M. Chen, J. A. Golovchenko, and D. Vanderbilt, *Phys. Rev. Lett.* **63**, 1257 (1989); P. Bedrossian, K. Mortensen, D. M. Chen, and J. A. Golovchenko, *Phys. Rev. B* **41**, 7545 (1990).
⁷I.-W. Lyo, Efthimios Kaxiras, and Ph. Avouris, *Phys. Rev. Lett.* **63**, 1261 (1989).
⁸H. Hibino, T. Fukuda, M. Suzuki, Y. Homma, T. Sato, M. Iwatsuki, K. Miki, and H. Tokumoto, *Phys. Rev. B* **47**, 13 027 (1993); K. Miki, Y. Morita, H. Tokumoto, T. Sato, M. Iwatsuki, M. Suzuki, and T. Fukuda, *Ultramicroscopy* **42-44**, 851 (1992).
⁹R. M. Feenstra and M. A. Lutz, *Phys. Rev. B* **42**, 5391 (1990); *Surf. Sci.* **243**, 151 (1991).
¹⁰R. T. Brockenbrough and J. W. Lyding, *Rev. Sci. Instrum.* **64**, 2225 (1993).
¹¹W. Kern, *Semicond. Int.* **7**, 94 (1984).
¹²R. S. Becker, J. A. Golovchenko, G. S. Higashi, and B. S. Swartzentruber, *Phys. Rev. Lett.* **57**, 1020 (1986).
¹³G.-X. Qian and D. J. Chadi, *J. Vac. Sci. Technol. B* **4**, 1079 (1986).
¹⁴R. S. Becker, B. S. Swartzentruber, J. S. Vickers, and T. Klitsner, *Phys. Rev. B* **39**, 1633 (1989).
¹⁵P. A. Bennett, M. Copel, D. Cahill, J. Falta, and R. M. Tromp, *Phys. Rev. Lett.* **69**, 1224 (1992).
¹⁶R. J. Wilson and S. Chiang, *Phys. Rev. Lett.* **58**, 2575 (1987).
¹⁷V. A. Tolomasov, V. V. Vaskin, M. I. Ovsyannikov, R. G. Loginova, and R. A. Rubtsova, *Fiz. Tekh. Poluprovodn.* **15**, 104 (1981) [*Sov. Phys. Semicond.* **15**, 61 (1981)].
¹⁸T. Hasegawa, M. Kohno, S. Hosaka, and S. Hosoki, *Phys. Rev. B* **48**, 1943 (1993); U. Kohler, J. E. Demuth, and R. J. Hamers, *J. Vac. Sci. Technol. A* **7**, 2860 (1989).
¹⁹John E. Northrup, *Phys. Rev. Lett.* **53**, 683 (1984).
²⁰Y.-N. Yang and E. D. Williams, *Phys. Rev. Lett.* **72**, 1862 (1994).

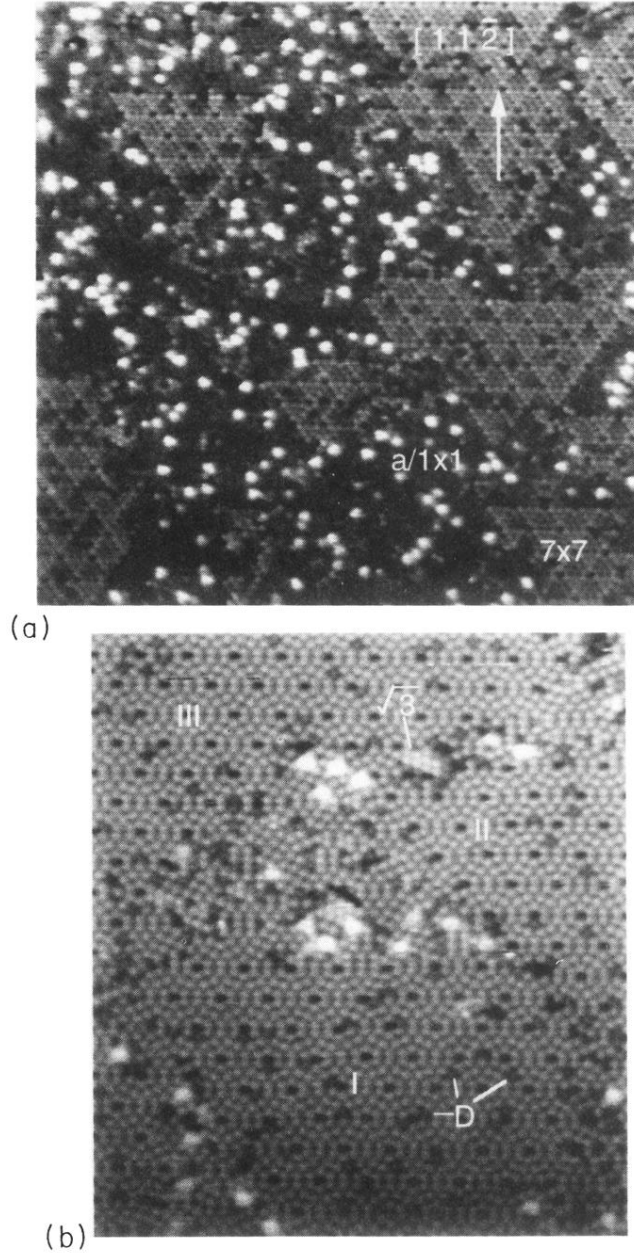


FIG. 1. STM images of a quenched Si(111) surface with high-B doping ($2 \times 10^{19}/\text{cm}^3$). (a) A $600 \times 600 \text{ \AA}^2$ occupied-state image taken at sample bias -1 V . The $a/1 \times 1$ regions appear darker. A patch of 7×7 bounded by faulted halves has grown in the middle of the $a/1 \times 1$ region. The area of $a/1 \times 1$ region is about 31%. (b) A $355 \times 400 \text{ \AA}^2$ unoccupied-state image taken at sample bias 1.5 V . A small triangular-shaped $a/1 \times 1$ region with a mixture of 2×2 , $c(4 \times 2)$, and $(\sqrt{3} \times \sqrt{3})R 30^\circ$ structures forms between the three domains of 7×7 (denoted by I, II, and III). The density of darker adatoms, marked by D , are about 0.5% in the 7×7 region.

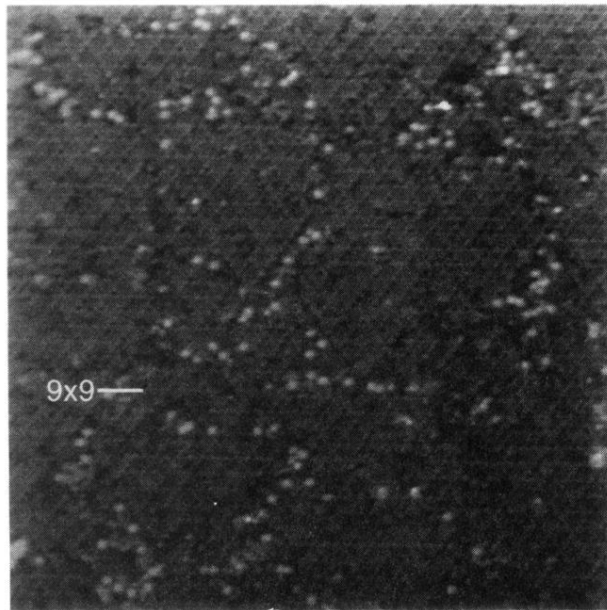


FIG. 2. A $800 \times 800\text{-}\text{\AA}^2$ STM image of a Si(111) surface with high-B doping ($2 \times 10^{19}/\text{cm}^3$) after flashing at 1280°C followed by annealing for 5 min at 560°C . The area of the $a/1 \times 1$ region is about 17%. A patch of 9×9 is visible.

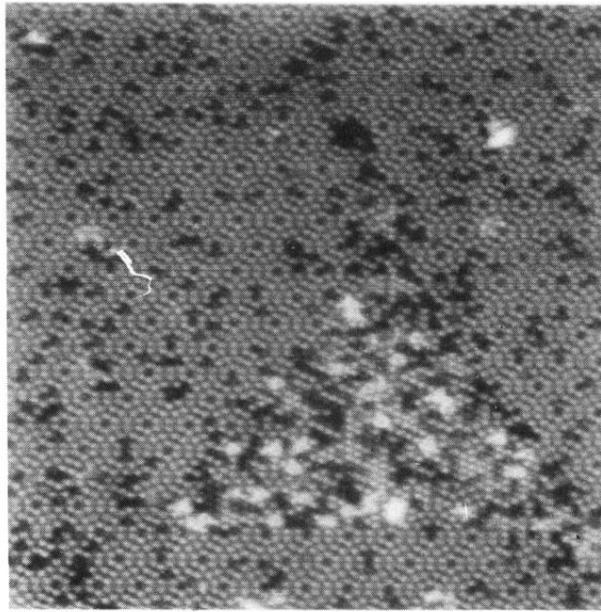


FIG. 3. A $450 \times 450 \text{-}\text{\AA}^2$ STM image of a Si(111) surface with high-B doping ($2 \times 10^{19}/\text{cm}^3$) after flashing at 1280°C followed by annealing for 2 min at 710°C . The $(\sqrt{3} \times \sqrt{3})R30^\circ$ structure is more pronounced in the triangular region. The area of $a/1 \times 1$ region is about 2.2%. The bright protrusions can be resolved into ringlike structures. The sample bias is +1 V.

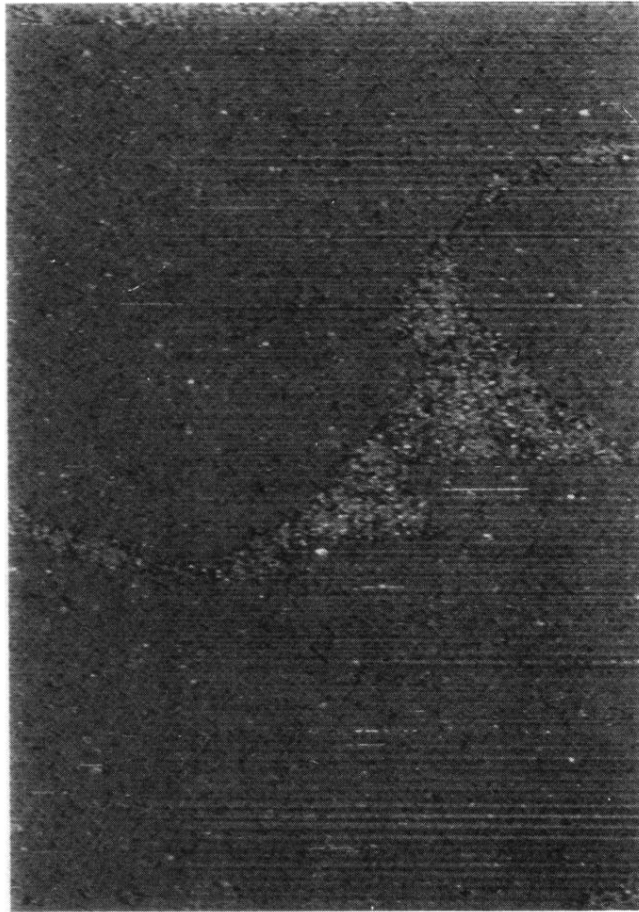


FIG. 4. A $2250 \times 3000\text{-}\text{\AA}^2$ STM image of a Si(111) surface with high-B doping ($2 \times 10^{19}/\text{cm}^3$) after flashing at 1280°C , followed by annealing for 2 min at 810°C . The sample bias is -1 V. The $a/1 \times 1$ regions (about 8.3% in area) have aggregated into larger regions surrounded by 7×7 domains.

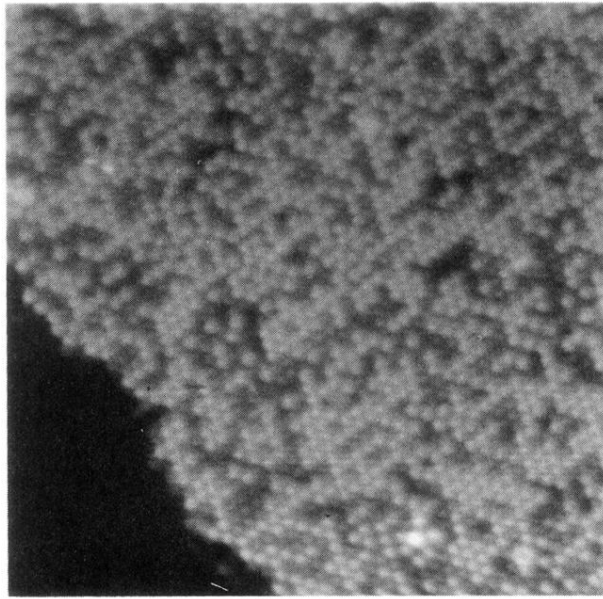


FIG. 5. A $300 \times 300 \text{-}\text{\AA}^2$ STM image of a Si(111) surface with high-B doping ($2 \times 10^{19}/\text{cm}^3$) after annealing for 1 h at 1280°C . The sample bias is +1 V. Domains of $(\sqrt{3} \times \sqrt{3})R30^\circ$ and $c(4 \times 2)$ and 2×2 are visible. The dark or bright adatoms of $(\sqrt{3} \times \sqrt{3})R30^\circ$ are believed to have B or Si, respectively, underneath them. The dark atoms occupy 5–8 % of the top bilayer atoms. The row pattern is discussed in Sec. IV B.

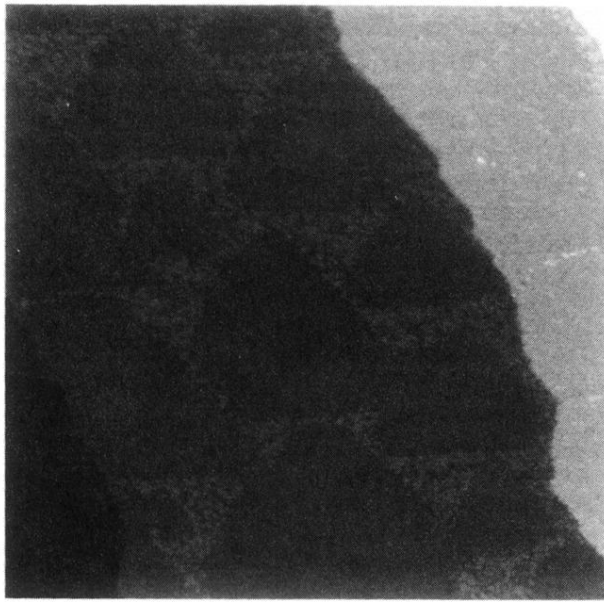


FIG. 7. A $2000 \times 2000 \text{-}\text{\AA}^2$ STM image of a Si(111) surface with high-B doping ($2 \times 10^{19}/\text{cm}^3$) after flashing at 1250°C followed by annealing for 3 min at 700°C . The sample bias is -2 V. The triangular-shaped 7×7 domains indicate that the growth of the 7×7 domains on this surface is along the three equivalent directions of $[11\bar{2}]$.